Two, three, or not to be? Elucidating Multiple Bonding in d^6 Pseudotetrahedral Oxo and Imide Complexes

Joel G. Gardner,† Joseph E. Schneider,† John S. Anderson*

Department of Chemistry, University of Chicago, Chicago, IL 60637, USA

ABSTRACT: Late transition metal oxo and imide complexes play an important role in the catalytic functionalization and activation of small molecules. An emerging theme in this area over the past few decades has been the use of lower-coordination numbers, and pseudo-tetrahedral geometries in particular, to stabilize what would otherwise be highly reactive species. However, the bonding structure in d^6 oxo and imide complexes in this geometry is ambiguous. These species are typically depicted with a triple bond, however recent experimental evidence suggests significant empirical differences between these complexes and other triply bonded complexes with lower d-counts. Here we use a suite of computational orbital localization methods and electron density analyses to probe the bonding structure of isoelectronic d^6 Co(III) oxo and imide complexes. These analyses suggest that a triple bond description is inaccurate due to a dramatically weakened σ interaction. While the exact bond order in these cases is necessarily dependent on the model used, several metrics suggest that the strength of the metal–O/N bond is most similar to other formally doubly bonded complexes.

Introduction

Late transition metal oxo and imide complexes are central intermediates in the functionalization and activation of small molecules.[1–6] The importance of these intermediates has motivated intense efforts at isolating and characterizing them to more thoroughly understand their properties and reactivity. However, the high d-electron counts in the late transition metals leads to weakening of the metal–oxygen or metal–nitrogen bond, which simultaneously enables much of their remarkable reactivity while making their isolation challenging.[6,7] One strategy which has been employed over the past few decades to enable the isolation of these species is moving to lower-coordination numbers, particularly in employing C_{3v} pseudotetetrahedral geometries. For instance, this strategy has enabled the recent isolation and characterization of several Co(III) imides and a Co(III) oxo complex.[5,8–16]

The C_{3v} symmetry of these complexes places the metal–oxo and metal–imide ("M–E") π-antibonding orbitals highest in energy within the d-manifold and, for low-spin complexes, thus allows for four d-electrons to populate metal centered M–E nonbonding orbitals of predominantly $d_{x^2-y^2}$ and d_{xy} character without significantly perturbing the M–E bond (Figure 1).[5,8,16] The lack of any π-antibonding electrons in this orbital picture suggests a triple-bond formulation in these complexes, consisting of one σ bond and two π bonds. Indeed this depiction is common in the literature.[8–10,13,14] However, it has also been suggested that a double bond is more appropriate.[15,17] This discrepancy comes from the question of whether to consider the σ-symmetry highest occupied molecular orbital (HOMO) as nonbonding or as antibonding. Formally, this orbital is expected to be the

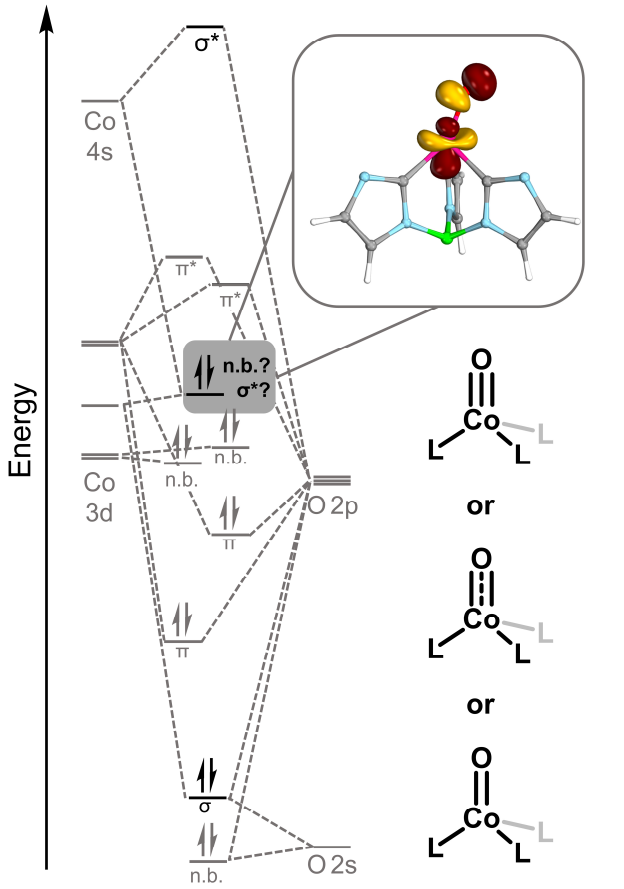

Figure 1. Qualitative MO diagram for the Co–O interaction in a C_{3v} symmetric d^6 oxo complex highlighting the d_{z^2}-derived HOMO of interest. The bond order in this case will be dependent on the nonbonding or antibonding character of this orbital. Phenyl and *tert*-butyl groups are omitted for clarity.

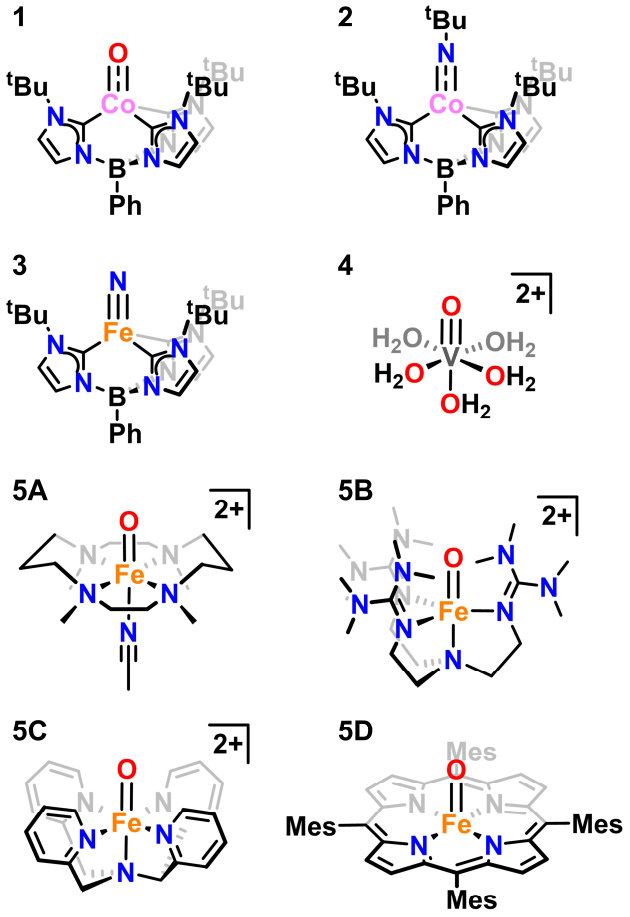

Chart 1. Complexes analyzed in this study.

antibonding combination of Co $3d_{z^2}$ and the E σ-donating orbital; i.e. an M–E σ* orbital. However, in C_{3v} symmetry $3d_{z^2}$ has the appropriate symmetry to hybridize with $4s$ and $4p_z$, which can impart some nonbonding character to the HOMO.[5] While it is generally acknowledged that the HOMO will carry some antibonding character, the general depiction of these complexes with triple bonds implies that the predominant character of this orbital is nonbonding.

This qualitative prediction of a partially nonbonding d_{z^2} orbital is supported by molecular orbital (MO) theory and DFT calculations on several systems.[5,17] However, experimentally probing the bond strength in many of the initially reported imide complexes is difficult as the Co–N stretching frequency of these imide complexes is convoluted by coupling with vibrations of their R-groups.[18] Oxo complexes do not have this complication, and indeed a recently isolated Co oxo complex (PhB(^{t}BuIm)$_3$Co^{III}O, Chart 1, **1**) enables determination of the Co–O stretching frequency. Interestingly, this frequency (815 cm^{-1}) is markedly lower than unambiguous examples of triply bonded oxo or nitride complexes,[10,19–22] indicating a lower bond order may be warranted. In fact, this value is much more reminiscent of formally doubly bonded Fe oxo complexes which exhibit stretches at 800-850 cm^{-1}.[23–27] This data stands on top of the observation that psuedotetrahedral Co^{III} oxo and imide complexes, as well as many related first-row d^6 examples, exhibit ~0.1 Å longer M–O/N bond lengths when compared with other bona fide examples of triply bonded complexes such as pseudotetrahedral Fe^{IV} nitride complexes.[7,19–21,28] This experimental data reveals that the bonding in these complexes is substantially weaker than that in other triply bonded examples. A double bond formulation would also be more consistent with bond orders typically drawn for d^6 oxo and imide complexes of second and third row transition metals in other four-coordinate geometries.[29–31] While bond orders can only imperfectly capture the complexities of a chemical bond, limiting bond order representations, such as double or triple bonds, imply different properties such as more nucleophilic or electrophilic reactivity respectively.[6] A careful reevaluation of the bond order in these complexes is therefore warranted, particularly given the unusual basic/nucleophilic reactivity observed in Co oxo **1**.[32]

To better understand the bonding in these complexes, we performed Natural Bond Orbital (NBO) and Intrinsic Bond Orbital (IBO) localizations and electron density analyses on the Co oxo complex **1** and an isoelectronic imide complex (PhB(^{t}BuIm)$_3$Co^{III}N^{t}Bu, Chart 1, **2**). The results obtained were compared to two previously experimentally characterized reference compounds with less ambiguous triple bonds – an analogous Fe nitride complex (PhB(^{t}BuIm)$_3$Fe^{IV}N, Chart 1, **3**) and the vanadyl ion ([(H$_2$O)$_5$V^{IV}O]$^{2+}$, Chart 1, **4**) – as well as a series of Fe oxo complexes which are assigned with formal Fe–O double bonds ([Fe^{IV}(O)(TMC)(NCCH$_3$)]$^{2+}$, [Fe^{IV}(O)(TMG$_3$tren)]$^{2+}$, [Fe^{IV}(O)(N4Py)]$^{2+}$, [Fe^{IV}(O)(TMP)]$^{2+}$, Chart 1, **5A-D**).[7,19,23–25,33] We find that the d_{z^2} based HOMOs of complexes **1** and **2** have significant antibonding character which makes a triple bond description inaccurate. While the assignment of a precise bond order between 2 and 3 will be highly dependent on the model employed, several metrics in this study, as well as experimentally determined stretching frequencies,[10,19,22–26] suggest the bond strength in these d^6 oxo and imide complexes is similar to that observed in formally doubly bonded Fe oxo complexes.

Results and Discussion

Complex Scope and Geometries

In order to obtain a more comprehensive picture of the bonding in these systems we chose a set of complexes which spanned d^6 species in pseudotetrahedral geometries (**1** and **2**) as well as reference complexes for canonical triple (**3**, and **4**) and double bonds (**5A-D**).[7,9,10,19,23–25,33] Each example shown in Chart 1 had its geometry optimized with DFT using the O3LYP functional and a local minimum was verified by frequency calculations. The computed structural parameters for each of these complexes match well with experimentally obtained data.[9,10,19,23–25,33,34] While the Fe oxo complexes will only be discussed in detail with regard to their bond order metrics, namely through delocalization indices (see below), complexes **1-4** were examined with a suite of analyses to understand the bonding in these species in greater detail.

Localization Analysis

We first used two localization methods, natural bond orbitals (NBOs) and intrinsic bond orbitals (IBOs), to convert the DFT-derived Kohn-Sham (KS) orbitals into

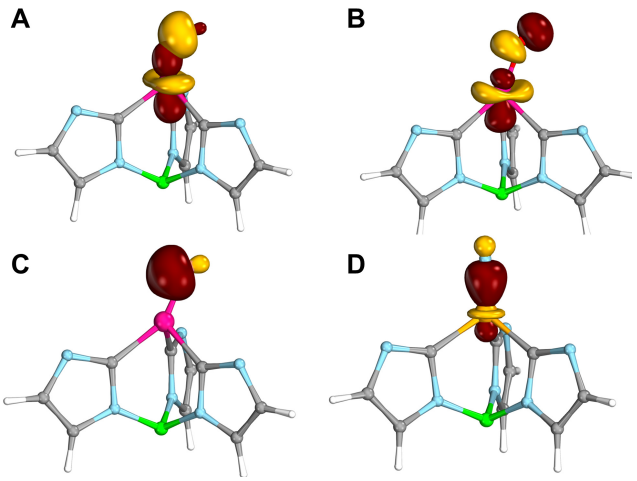

Figure 2. An antibonding combination of NBO localized Co and O lone pairs of **1** (A), the Kohn-Sham (KS) HOMO of **1** (B), the IBO-localized σ-bonding orbital of **1** (C), and that of the Fe nitride complex **3** (D). Phenyl and tert-butyl groups are omitted for clarity.

more localized bonding, antibonding, and nonbonding orbitals. NBO analysis aims to partition electron density into an optimal Lewis diagram.[35,36] The default NBO localization settings assign double bonds to the Co oxo complex **1** and the Co imide complex **2** and triple bonds to the Fe nitride complex **3** and the V oxo complex **4**. By itself, this analysis indicates a double bond is at the very least a competitive assignment for the Co–O bond in **1** and the Co–N bond in **2**. Interestingly, while the Fe nitride complex **3** and the V oxo complex **4** both contain a clear σ-bonding metal–O/N orbital, neither Co complex includes one (Figures S1–S5). In the Co imide complex **2**, the two Co–N bonding orbitals which are found are of clear π-symmetry. In lieu of a σ-bond there are overlapping σ-symmetry lone pairs on Co and N (Figure S3). The Co–O bond in **1** is more complicated, as one of the bonding orbitals lacks the axial symmetry necessary to clearly label it as σ or π. However, as in **2**, complex **1** has lone pairs on both Co and O which overlap. The antibonding combination of these lone pairs strongly resembles the KS-HOMO of **1**, supporting that the HOMO weakens the σ-bonding interaction (Figure 2A and B). Furthermore, for both Co oxo **1** and Co imide **2** these lone pairs on Co are 99% 3*d*-orbital, 1% 4*s*-orbital, and the total natural population of the Co 4*s* orbital is 0.3 electrons (See table S3). No higher lying orbital with greater 4*s* character is a major contributor to the KS-HOMOs of either Co oxo **1** or Co imide **2**. Together, these observations suggest hybridization between the 3*d* and 4*s* Co orbitals is minimal, further supporting a σ* interaction in the HOMO.

For the Co imide **2**, NBO localized a low-lying vacant orbital which is 99% 4*s* based, allowing a more detailed assessment of this orbital's interactions with other orbitals via second order perturbation analysis. This analysis quantifies the stabilization due to small amounts of mixing between low lying and high lying orbitals in the NBO basis. By this analysis, the 4*s* orbital of Co imide **2** has a substantial interaction of 56 kcal/mol with the $3d_{z^2}$-derived Co lone pair and an interaction of 21 kcal/mol with the N lone pair. The only other significant interactions with this orbital (those > 2 kcal/mol) are an interaction of 4 kcal/mol with the N–C bond in the imide and an interaction of 26-27 kcal/mol with each of the carbene donor lone pairs. Thus, despite the lack of a third bonding orbital between Co and N and little mixing between the 3*d* and 4*s* orbital, the 4*s* orbital nonetheless greatly stabilizes the Co imide **2**. NBO does not localize a similar unoccupied orbital for the Co oxo **1**, however if C_{3V} symmetry about the Co–O bond is enforced by restricting the B–Co–O bond to 180°, such an orbital is found. The interactions of this 4*s* orbital of the linearized Co oxo **1** are similar to those of the Co imide **2**: An interaction of 42 kcal/mol with the Co $3d_{z^2}$, interactions of 27 kcal/mol and 4 kcal/mol with the two O lone pairs, and interactions of 34-35 kcal/mol with the carbene donor lone pairs. Thus, while NBO analysis suggests a double bond formalism with little hybridization for both of the Co oxo **1** and Co imide **2** complexes, significant stabilization from mixing with the 4*s* orbital are also evident. These conflicting results suggest that an intermediate bond order may be most appropriate, and furthermore motivate the analysis of the bonds in these molecules via other techniques.

IBO analysis is an alternative localization scheme that concentrates an orbital's electron population on as few atoms as possible.[37,38] For both Co complexes **1** and **2**, IBO localization generates three occupied Co–O/N bonding orbitals. However, in both cases the σ-bonding orbital is heavily polarized and resembles a lone pair on the ligand (Figure 2C, S6, and S7), resulting in less electron density localized in the internuclear region than in a typical σ-bonding orbital. This is a significant departure from the corresponding metal–O/N σ-orbital in both benchmark complexes **3** and **4**, which is more evenly shared between the metal and the ligand (Figure 2D, S9, and S10). Such extreme polarization is not seen in the metal–O/N π-bonding orbitals of any complex (Figures S6, S7, S9, and S10).

Similar to NBO localization, IBO localization also finds a highly axially asymmetric Co–O bonding orbital for the Co oxo complex **1**, likely arising from the observed distortion away from C_{3v} symmetry by bending of the B–Co–O angle. We further investigated this by reoptimizing the complex with the B–Co–O angle restricted to a series of values between the equilibrium 158° and the idealized 180°. As this oxo bond is "straightened", the axially asymmetric orbital transforms into a π-bonding orbital (Figure S8) and its energy increases. Thus, it appears that the distortion of **1** out of C_{3v} symmetry strengthens one of the Co–O π-bonds. However, this is energetically offset by changes to other orbitals, including the Co–O σ-interaction, which have a net destabilizing effect. The overall DFT-derived energy changes by less than 1 kcal/mol upon linearization, indicating that the bond strength is not substantially altered on the whole (Table S1).

The conclusion from these localization assays of the bonding in the d^6 Co complexes **1** and **2** is that assigning the Co–O/N bonds as triple bonds is too simplistic. NBO localization predicts only two bonding orbitals in both complexes, and neither of these orbitals represents a canonical σ-bond as observed in the reference complexes **3** and **4**. Similarly, IBO localization supports two bonding interactions and a highly polar σ-interaction which resembles an oxygen lone pair. Qualitatively, these analyses

Table 1. Atoms in Molecules bonding metrics.

	1	2	3	4
ρ_{CP}[a]	0.203	0.202	0.345	0.307
ϵ_{CP}[b]	0.054	0.006	0.002	0.007

[a]Electron density at the critical point (a.u.) as defined by Atoms In Molecules. [b]Ellipticity of the electron density at the critical point (dimensionless) as defined by Atoms In Molecules.

are consistent with the picture suggested by molecular orbital theory and previous assumptions about the bonding in these complexes, namely that there should be a weakened but not entirely absent σ interaction due to antibonding contributions. However, the localized orbitals have σ-interactions which are quite weak, and this is more consistent with the assignment of **1** and **2**'s HOMO as predominantly, not partially, σ-antibonding.

Electron Density Analysis

We next turned to analysis of the electronic density for further insight into the nature of the bonding interaction in these complexes.[39] Bader's theory of Atoms in Molecules (AIM) provides a means of partitioning atoms and locating bonds in real space based on the gradient of the electron density. The boundary between atoms is positioned such that the electron density is at a minimum as the boundary is crossed. The position of maximum electron density on the boundary between two bonded atoms is called the bond critical point, ρ_{CP}, and the electron density at this point can be used to characterize the strength of the bond. Stronger bonds tend to have more electron density at their bond critical point, and asymmetry in the curvature of the maxima within the boundary – the ellipticity, ϵ_{CP} – differentiates between an odd and even number of π interactions.[40,41]

AIM analysis of both Co complexes **1** and **2** show a significant reduction in electron density compared with the benchmark complexes **3** and **4** at their respective metal–O/N bond critical points indicating weaker bonds (Table 1, Figure 3, Table 2). Furthermore, these same critical points have ellipticity values close to zero, indicating a cylindrically symmetric distribution of charge for all four complexes. This is consistent with there being two π-bonds between the metal and O/N ligands.[40,41] While the Co oxo complex **1** does have a higher ellipticity than the other complexes, the value is still an order of magnitude lower than those observed in canonical double bonds; the ellipticity of the C–C bond in ethylene is 0.298.[41] This further supports that the geometric distortion from linearity in **1** does not substantially affect the nature of the Co–O bond. Taken together, the critical point electron densities and ellipticities show that while the Co–O/N bonds in complexes **1** and **2** have the symmetry of a triple bond, they are weaker than canonical triple bonds. To the extent that bond strength and bond order are related this means the Co–O/N bond orders in **1** and **2** are lower than the metal–O/N bond orders in complexes **3** and **4**.

Delocalization Indices

Higher bond orders are associated with more shared electron pairs, and the number of electron pairs shared between two atoms can be estimated with the delocalization index (DI). The computation of DI depends on the method used to assign physical space to different atoms.[39] Bader's partitioning is that of Atoms in Molecules described above, in which the topology of the electron density is used to rigidly draw boundaries between different atoms. There are also methods which draw so-called fuzzy boundaries in which atoms share points in space as defined by weighting function; two such methods are those of Becke and Hirshfeld which use atomic radii and free atomic electron densities, respectively, to determine the weighting functions.[42,43] Finally, it is also possible to divide up atomic space based on atomic orbitals instead of physical space; the Mayer bond order does just this with the Mulliken partitioning of orbital space,[44] and the NAO-Wiberg bond order does this with the natural atomic orbitals from NBO analysis.

We find that within all definitions of atomic space there are fewer electron pairs shared between Co and O/N in **1** and **2** than between Fe/V and N/O in **3** and **4** (Table 2). We note in particular the delocalization index integrated in Becke fuzzy atomic space ("fuzzy delocalization index", or f-DI), recovers values close to three electron pairs for the canonical triple metal–O/N bonds in **3** and **4**. In contrast, the Co oxo complex **1** and Co imide complex **2** both have substantially lower f-DI values closer to two electron pairs (Table 2). This analysis indicates fewer electrons are effectively shared across the Co–O/N bonds of **1** and **2** than across the metal–O/N bonds of **3** and **4**.

The impact of the individual orbitals on this bond order metric can be specifically analyzed by the Molecular Orbital Delocalization Index (MO-DI) which breaks the delocalization index into orbital contributions.[45] This breakdown considers both the delocalization within each orbital (diagonal elements) as well as the interference between orbitals (off-diagonal elements) which can be either constructive or destructive.

MO-DI corroborates the assignment of the HOMO of the Co oxo complex **1** as having significant antibonding character.

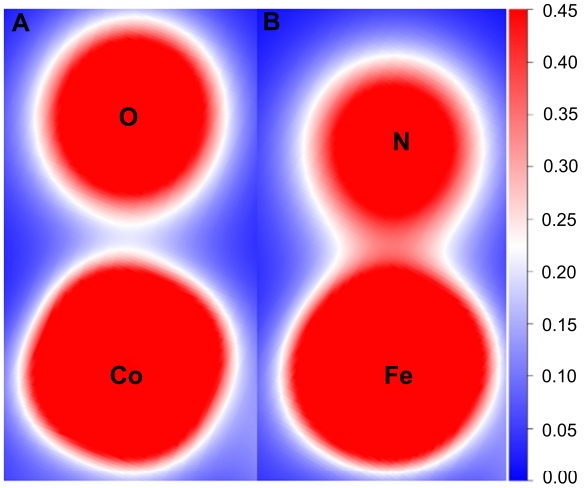

Figure 3. Electron Density of **1** (A) and **3** (B), in a plane containing the M-E bond.

Table 2. Delocalization indices computed in various definitions of atomic space

	1	2	3	4	5a	5b	5c	5d
Becke	2.28	2.35	3.02	2.91	2.37	2.40	2.40	2.44
Hirshfeld	1.94	2.02	2.94	2.68	2.12	2.20	2.20	2.34
Bader	1.43	1.69	2.49	2.03	1.72	1.70	1.74	1.79
Mayer	1.41	1.84	2.80	2.42	2.06	1.91	1.97	2.06
NAO-Wiberg	0.93	1.20	2.13	2.13	1.51	1.53	1.56	1.62

The sum of the diagonal and off-diagonal elements associated with the KS-HOMO of **1** corresponds to a decrease of 0.34 electron pairs shared between Co and O, which is 54% of the difference between the f-DI of the Co–O bond of **1** and the V–O bond of **4**. This orbital interacts most strongly with an orbital which is σ-bonding with respect to Co and O (Figure S11), with an off-diagonal destructive interference of –0.36 electron pairs. The antibonding character in the HOMO of **1** and the resultant destabilization of the σ-bond are both corroborated by this method.

The remainder of the difference between the f-DIs of the Co–O bond of **1** and the V–O bond of **4** primarily comes from the formally nonbonding orbitals immediately below the HOMO of **1**. The total effects of the KS-HOMO–1 and KS-HOMO–2 orbitals are decreases in 0.11 electron pairs and 0.09 electron pairs, respectively, due to destructive interference with orbitals of π symmetry (Figure S11). Surprisingly, this implies these formally Co–O nonbonding orbitals have some π-antibonding character. This is likely due to the idealized C_{3v} symmetry of the complex, in which the nonbonding orbitals have the same symmetry as π-orbitals. Collectively, the KS-HOMO, KS-HOMO–1, and KS-HOMO–2 in **1** account for 86% of the difference between the Co–O bond of **1** and the V–O bond of **4**, with the primary contributor to the weaker bond in **1** being the antibonding character in the KS-HOMO.

The same MO-DI analysis shows a much smaller effect when applied to the frontier orbitals of the Co imide complex **2**. Collectively, **2**'s KS-HOMO, KS-HOMO–1, and KS-HOMO–2 decrease the f-DI by 0.08 electron pairs. The most destabilizing individual orbital of these three is the KS-HOMO-2, which removes 0.05 electron pairs from the f-DI. In fact, no particular orbital appears to be the dominant reason for the decreased f-DI of **2** relative to the canonical triple bonds in **3** and **4**. A further difference between the KS-orbitals of **1** and the KS-orbitals of **2** is the placement of the d_{z^2}-derived orbital; while in **1** this orbital is found as the HOMO as predicted by MO theory, for **2** the KS-orbital most resembling d_{z^2} is the HOMO–2 (Figure S12). We believe these differences are due to ^{t}Bu character in the frontier KS-orbitals in **2**, which could prevent the bonding and antibonding interactions from being concentrated in individual orbitals. Such an explanation is consistent with the similarities in the NBO and IBO localized orbitals of Co oxo complex **1** and Co imide complex **2** (see above) as well as their similar overall f-DI.

The low delocalization indices of the Co–N/O bonds in complexes **1** and **2** is further evidence that these bonds are not full triple bonds and raises the question of whether these cases are better defined as double bonds. To further examine this possibility we analyzed several Fe(IV) oxo complexes which are generally understood to have double bonds (Chart 1, **5A**-**D**).[23–25,33] Notably, all of these complexes have larger delocalization indices than the Co complexes **1** and **2** with any definition used. No definition of atomic space gives precise integer values as would be expected for classic double or triple metal–O/N bond orders in complexes **3**-**5**, cautioning against using delocalization to make a precise, quantitative assignment of the metal–O/N bond order. However, this analysis does demonstrate that the Co–O/N bonds in **1** and **2** resemble double bonds more than triple bonds, at least by these metrics.

Conclusion

The analyses compiled in this work collectively indicate that the Co–N and Co–O bonds in pseudotetrahedral Co(III) imide and oxo complexes are fundamentally distinct from canonical metal–O/N triple bonds. NBO and IBO analyses demonstrate the σ-electrons in the Co oxo complex **1** and the Co imide complex **2** can be well-approximated as lone pairs, in dramatic contrast to the evenly shared metal–O/N σ-bonding orbitals in benchmark triply bonded complexes **3** and **4**. Electron density analysis reveals a lower critical point electron density at the metal–O/N bond critical points of **1** and **2** when compared to **3** and **4**, providing further evidence of weaker bonding. Delocalization indices of the Co–O/N bonds of **1** and **2** and vibrational data of the former provide a clearer picture that the bonding is more similar to double Fe–O bonds in complexes **5A**-**D** than to the metal–O/N triple bonds of **3** and **4**. For the Co oxo complex **1**, this is rationalized by clear antibonding character in the HOMO leading to weakened σ-bonding, although it is likely that weakened Co–O π-bonding plays a small role as well.

The picture that emerges is consistent with MO theory, in which limited hybridization prevents the d_{z^2} orbital from taking on full antibonding character. However, our analyses here argue that the stabilization gained from hybridization is minimal, and that the HOMO orbital maintains predominant antibonding character. While the individual orbital contributions to the Co imide complex **2** are less clear, the properties of the bonds as a whole are sufficiently similar that assigning significantly different bonding pictures to the two bonds seems unreasonable. While our conclusions here are only firmly tethered to the set complexes we have examined, our results imply that similarly lower bond orders may be present in related imide complexes.

Altogether, our calculations are inconsistent with assigning the Co–O/N bond in complexes **1** and **2** as a triple bond. Such an assignment overstates the strength of the bond and the extent of electron pair sharing within it. It is less clear that the evidence is strong enough to confidently label these

bonding interactions as double bonds, however several metrics, including experimental vibrational data, suggest this assignment could be reasonable. Ultimately, there is little merit in debating a precise fractional bond order describing the interactions in these complexes. Nonetheless, all analyses point towards a double bond as being a closer reflection of the electronic properties of these interactions, and at the very least rule out a triple bond as an accurate representation.

Methodology

Geometry optimizations were performed in Orca 4.1 using the O3LYP functional.[46–48] The resolution of identity approximation was used for coulomb integrals and the chain of spheres approximation was used for exchange integrals. The initial geometry for complexes **1**, **5a**, **5b**, and **5c** were taken from the literature.[10,25,49,50] The initial geometries for all other complexes (**2**, **3**, **4,** and **5d**) were generated in Avogadro 1.90.0.[51,52] Calculations used the def2-TZVPP basis set on the metal atom, the def2-TZVP basis set on all atoms bonded to the metal atom, and the def2-SV(P) basis set on all other atoms.[53,54] A solvent correction is incorporated via the conductor-like polarizable continuum model with the dielectric constant of acetonitrile. Optimization to stable minima was confirmed via analytical frequencies calculations. All analyses were then performed on the Kohn-Sham wavefunction similarly calculated at the equilibrium geometry. NBO Analysis was performed with NBO 6.0 and the orbitals visualized in their pre-orthogonalized form.[36] IBO calculations were performed in IboView V20150427,[38] with the IBO (Exponent 4) chemical analysis function used to generate the localized orbitals. Multiwfn 3.8 was used for electron density analysis, delocalization index calculations, and wavefunction input conversions.[39] While there is little theoretical support for the use of Kohn-Sham wavefunctions for calculating delocalization indices, in practice there is little difference between delocalization indices calculated by DFT and those calculated by WFT.[55]

ASSOCIATED CONTENT

Supporting Information. Additional NBO and IBO orbital figures for all complexes, electron density metrics, Co oxo B–Co–O angle scan energies and IBO figures, details of MO-DI, and optimized geometries. This material is available free of charge via the Internet at http://pubs.acs.org.

AUTHOR INFORMATION

Corresponding Author

*jsanderson@uchicago.edu

Author Contributions

†These authors contributed equally. The manuscript was written through contributions of all authors. All authors have given approval to the final version of the manuscript.

Notes

The authors declare no competing financial interest.

ACKNOWLEDGMENT

This work was funded by the National Science Foundation (1654144), and the University of Chicago. Computations were generously supported by the UChicago Research Computing Center. J.E.S. thanks the Department of Defense for a National Defense and Engineering Graduate Fellowship (00003765), and J.S.A. thanks the Sloan Foundation for a Research Fellowship (FG-2019-11497). We also thank Professor Gerald Knizia for technical assistance in IBO Analysis.

REFERENCES

(1) Zhang, W.; Lai, W.; Cao, R. Energy-Related Small Molecule Activation Reactions: Oxygen Reduction and Hydrogen and Oxygen Evolution Reactions Catalyzed by Porphyrin- and Corrole-Based Systems. *Chem. Rev.* **2017**, *117* (4), 3717–3797. https://doi.org/10.1021/acs.chemrev.6b00299.

(2) Artero, V.; Chavarot-Kerlidou, M.; Fontecave, M. Splitting Water with Cobalt. *Angew. Chem. Int. Ed.* **2011**, *50* (32), 7238–7266. https://doi.org/10.1002/anie.201007987.

(3) Eikey, R. Nitrido and Imido Transition Metal Complexes of Groups 6–8. *Coord. Chem. Rev.* **2003**, *243* (1–2), 83–124. https://doi.org/10.1016/S0010-8545(03)00048-1.

(4) Gunay, A.; Theopold, K. H. C−H Bond Activations by Metal Oxo Compounds. *Chem. Rev.* **2010**, *110* (2), 1060–1081. https://doi.org/10.1021/cr900269x.

(5) Saouma, C. T.; Peters, J. C. ME and ME Complexes of Iron and Cobalt That Emphasize Three-Fold Symmetry (E=O, N, NR). *Coord. Chem. Rev.* **2011**, *255* (7–8), 920–937. https://doi.org/10.1016/j.ccr.2011.01.009.

(6) Gray, H. B.; Winkler, J. R. Living with Oxygen. *Acc. Chem. Res.* **2018**, *51* (8), 1850–1857. https://doi.org/10.1021/acs.accounts.8b00245.

(7) Ballhausen, C. J.; Gray, H. B. The Electronic Structure of the Vanadyl Ion. *Inorg. Chem.* **1962**, *1* (1), 111–122. https://doi.org/10.1021/ic50001a022.

(8) Jenkins, D. M.; Betley, T. A.; Peters, J. C. Oxidative Group Transfer to Co(I) Affords a Terminal Co(III) Imido Complex. *J. Am. Chem. Soc.* **2002**, *124* (38), 11238–11239. https://doi.org/10.1021/ja026852b.

(9) Cowley, R. E.; Bontchev, R. P.; Sorrell, J.; Sarracino, O.; Feng, Y.; Wang, H.; Smith, J. M. Formation of a Cobalt(III) Imido from a Cobalt(II) Amido Complex. Evidence for Proton-Coupled Electron Transfer. *J. Am. Chem. Soc.* **2007**, *129* (9), 2424–2425. https://doi.org/10.1021/ja066899n.

(10) Goetz, M. K.; Hill, E. A.; Filatov, A. S.; Anderson, J. S. Isolation of a Terminal Co(III)-Oxo Complex. *J. Am. Chem. Soc.* **2018**, *140* (41), 13176–13180. https://doi.org/10.1021/jacs.8b07399.

(11) Shay, D. T.; Yap, G. P. A.; Zakharov, L. N.; Rheingold, A. L.; Theopold, K. H. Intramolecular C?H Activation by an Open-Shell Cobalt(III) Imido Complex. *Angew. Chem. Int. Ed.* **2005**, *44* (10), 1508–1510. https://doi.org/10.1002/anie.200462529.

(12) Liu, Y.; Du, J.; Deng, L. Synthesis, Structure, and Reactivity of Low-Spin Cobalt(II) Imido Complexes [(Me $_3$ P) $_3$ Co(NAr)]. *Inorg. Chem.* **2017**, *56* (14),

8278–8286. https://doi.org/10.1021/acs.inorgchem.7b00941.

(13) Ray, K.; Heims, F.; Pfaff, F. F. Terminal Oxo and Imido Transition-Metal Complexes of Groups 9-11. *Eur. J. Inorg. Chem.* **2013**, *2013* (22–23), 3784–3807. https://doi.org/10.1002/ejic.201300223.

(14) Dai, X.; Kapoor, P.; Warren, T. H. [Me $_2$ NN]Co(η ^{6} -Toluene): OO, NN, and ON Bond Cleavage Provides β-Diketiminato Cobalt μ-Oxo and Imido Complexes. *J. Am. Chem. Soc.* **2004**, *126* (15), 4798–4799. https://doi.org/10.1021/ja036308i.

(15) Hu, X.; Meyer, K. Terminal Cobalt(III) Imido Complexes Supported by Tris(Carbene) Ligands: Imido Insertion into the Cobalt−Carbene Bond. *J. Am. Chem. Soc.* **2004**, *126* (50), 16322–16323. https://doi.org/10.1021/ja044271b.

(16) Larson, V. A.; Battistella, B.; Ray, K.; Lehnert, N.; Nam, W. Iron and Manganese Oxo Complexes, Oxo Wall and Beyond. *Nat Rev Chem* **2020**, *4* (8), 404–419. https://doi.org/10.1038/s41570-020-0197-9.

(17) Wasbotten, I. H.; Ghosh, A. Spin-State Energetics and Spin-Crossover Behavior of Pseudotetrahedral Cobalt(III)–Imido Complexes. The Role of the Tripodal Supporting Ligand. *Inorg. Chem.* **2007**, *46* (19), 7890–7898. https://doi.org/10.1021/ic700543f.

(18) Mehn, M. P.; Brown, S. D.; Jenkins, D. M.; Peters, J. C.; Que, L. Vibrational Spectroscopy and Analysis of Pseudo-Tetrahedral Complexes with Metal Imido Bonds. *Inorg. Chem.* **2006**, *45* (18), 7417–7427. https://doi.org/10.1021/ic060670r.

(19) Scepaniak, J. J.; Fulton, M. D.; Bontchev, R. P.; Duesler, E. N.; Kirk, M. L.; Smith, J. M. Structural and Spectroscopic Characterization of an Electrophilic Iron Nitrido Complex. *J. Am. Chem. Soc.* **2008**, *130* (32), 10515–10517. https://doi.org/10.1021/ja8027372.

(20) Rohde, J.-U.; Betley, T. A.; Jackson, T. A.; Saouma, C. T.; Peters, J. C.; Que, L. XAS Characterization of a Nitridoiron(IV) Complex with a Very Short Fe–N Bond. *Inorg. Chem.* **2007**, *46* (14), 5720–5726. https://doi.org/10.1021/ic700818q.

(21) Groves, J. T.; Kruper, W. J.; Haushalter, R. C.; Butler, W. M. Synthesis, Characterization, and Molecular Structure of Oxo(Porphyrinato)Chromium(IV) Complexes. *Inorg. Chem.* **1982**, *21* (4), 1363–1368. https://doi.org/10.1021/ic00134a018.

(22) Evans, J. C. The Vibrational Spectra and Structure of the Vanadyl Ion in Aqueous Solution. *Inorg. Chem.* **1963**, *2* (2), 372–375. https://doi.org/10.1021/ic50006a031.

(23) Rohde, J.-U. Crystallographic and Spectroscopic Characterization of a Nonheme Fe(IV)&cjs0811;O Complex. *Science* **2003**, *299* (5609), 1037–1039. https://doi.org/10.1126/science.299.5609.1037.

(24) Wang, D.; Ray, K.; Collins, M. J.; Farquhar, E. R.; Frisch, J. R.; Gómez, L.; Jackson, T. A.; Kerscher, M.; Waleska, A.; Comba, P.; Costas, M.; Que, L. Nonheme Oxoiron(IV) Complexes of Pentadentate N5 Ligands: Spectroscopy, Electrochemistry, and Oxidative Reactivity. *Chem. Sci.* **2013**, *4* (1), 282–291. https://doi.org/10.1039/C2SC21318D.

(25) England, J.; Martinho, M.; Farquhar, E. R.; Frisch, J. R.; Bominaar, E. L.; Münck, E.; Que, L. A Synthetic High-Spin Oxoiron(IV) Complex: Generation, Spectroscopic Characterization, and Reactivity. *Angew. Chem. Int. Ed.* **2009**, *48* (20), 3622–3626. https://doi.org/10.1002/anie.200900863.

(26) England, J.; Guo, Y.; Van Heuvelen, K. M.; Cranswick, M. A.; Rohde, G. T.; Bominaar, E. L.; Münck, E.; Que, L. A More Reactive Trigonal-Bipyramidal High-Spin Oxoiron(IV) Complex with a Cis-Labile Site. *J. Am. Chem. Soc.* **2011**, *133* (31), 11880–11883. https://doi.org/10.1021/ja2040909.

(27) Hong, S.; So, H.; Yoon, H.; Cho, K.-B.; Lee, Y.-M.; Fukuzumi, S.; Nam, W. Reactivity Comparison of High-Valent Iron(Iv)-Oxo Complexes Bearing N-Tetramethylated Cyclam Ligands with Different Ring Size. *Dalton Trans.* **2013**, *42* (22), 7842. https://doi.org/10.1039/c3dt50750e.

(28) Hong, S.; Lee, Y.-M.; Sankaralingam, M.; Vardhaman, A. K.; Park, Y. J.; Cho, K.-B.; Ogura, T.; Sarangi, R.; Fukuzumi, S.; Nam, W. A Manganese(V)–Oxo Complex: Synthesis by Dioxygen Activation and Enhancement of Its Oxidizing Power by Binding Scandium Ion. *J. Am. Chem. Soc.* **2016**, *138* (27), 8523–8532. https://doi.org/10.1021/jacs.6b03874.

(29) Delony, D.; Kinauer, M.; Diefenbach, M.; Demeshko, S.; Würtele, C.; Holthausen, M. C.; Schneider, S. A Terminal Iridium Oxo Complex with a Triplet Ground State. *Angew. Chem. Int. Ed.* **2019**, *58* (32), 10971–10974. https://doi.org/10.1002/anie.201905325.

(30) Kinauer, M.; Diefenbach, M.; Bamberger, H.; Demeshko, S.; Reijerse, E. J.; Volkmann, C.; Würtele, C.; van Slageren, J.; de Bruin, B.; Holthausen, M. C.; Schneider, S. An Iridium(III / IV / V) Redox Series Featuring a Terminal Imido Complex with Triplet Ground State. *Chem. Sci.* **2018**, *9* (18), 4325–4332. https://doi.org/10.1039/C8SC01113C.

(31) Poverenov, E.; Efremenko, I.; Frenkel, A. I.; Ben-David, Y.; Shimon, L. J. W.; Leitus, G.; Konstantinovski, L.; Martin, J. M. L.; Milstein, D. Evidence for a Terminal Pt(Iv)-Oxo Complex Exhibiting Diverse Reactivity. *Nature* **2008**, *455* (7216), 1093–1096. https://doi.org/10.1038/nature07356.

(32) Goetz, M. K.; Anderson, J. S. Experimental Evidence for p K_a -Driven Asynchronicity in C–H Activation by a Terminal Co(III)–Oxo Complex. *J. Am. Chem. Soc.* **2019**, *141* (9), 4051–4062. https://doi.org/10.1021/jacs.8b13490.

(33) Fertinger, C.; Hessenauer-Ilicheva, N.; Franke, A.; van Eldik, R. Direct Comparison of the Reactivity of Model Complexes for Compounds 0, I, and II in Oxygenation, Hydrogen-Abstraction, and Hydride-Transfer Processes. *Chemistry - A European Journal* **2009**, *15* (48), 13435–13440. https://doi.org/10.1002/chem.200901804.

(34) Krakowiak, J.; Lundberg, D.; Persson, I. A Coordination Chemistry Study of Hydrated and Solvated Cationic Vanadium Ions in Oxidation States +III, +IV, and +V in Solution and Solid State. *Inorg.*

Chem. **2012**, *51* (18), 9598–9609. https://doi.org/10.1021/ic300202f.

(35) Glendening, E. D.; Landis, C. R.; Weinhold, F. Natural Bond Orbital Methods. *WIREs Comput Mol Sci* **2012**, *2* (1), 1–42. https://doi.org/10.1002/wcms.51.

(36) NBO 6.0. E. D. Glendening, J. K. Badenhoop, A. E. Reed, J. E. Carpenter, J. A. Bohmann, C. M. Morales, C. R. Landis, and F. Weinhold (Theoretical Chemistry Institute, University of Wisconsin, Madison, WI, 2013); Http://Nbo6.Chem.Wisc.Edu/.

(37) Knizia, G. Intrinsic Atomic Orbitals: An Unbiased Bridge between Quantum Theory and Chemical Concepts. *J. Chem. Theory Comput.* **2013**, *9* (11), 4834–4843. https://doi.org/10.1021/ct400687b.

(38) Knizia, G.; Klein, J. E. M. N. Electron Flow in Reaction Mechanisms-Revealed from First Principles. *Angew. Chem. Int. Ed.* **2015**, *54* (18), 5518–5522. https://doi.org/10.1002/anie.201410637.

(39) Lu, T.; Chen, F. Multiwfn: A Multifunctional Wavefunction Analyzer. *J. Comput. Chem.* **2012**, *33* (5), 580–592. https://doi.org/10.1002/jcc.22885.

(40) Bader, R. F. W.; Matta, C. F.; Cortés-Guzmán, F. Where To Draw the Line in Defining a Molecular Structure. *Organometallics* **2004**, *23* (26), 6253–6263. https://doi.org/10.1021/om049450g.

(41) Popelier, P. L. *Atoms in Molecules: An Introduction*; 2009.

(42) Becke, A. D. A Multicenter Numerical Integration Scheme for Polyatomic Molecules. *J. Chem. Phys.* **1988**, *88* (4), 2547–2553. https://doi.org/10.1063/1.454033.

(43) Hirshfeld, F. L. Bonded-Atom Fragments for Describing Molecular Charge Densities. *Theoret. Chim. Acta* **1977**, *44* (2), 129–138. https://doi.org/10.1007/BF00549096.

(44) Matito, E.; Poater, J.; Solà, M.; Duran, M.; Salvador, P. Comparison of the AIM Delocalization Index and the Mayer and Fuzzy Atom Bond Orders. *J. Phys. Chem. A* **2005**, *109* (43), 9904–9910. https://doi.org/10.1021/jp0538464.

(45) de Lange, J. H.; van Niekerk, D. M. E.; Cukrowski, I. Quantifying Individual (Anti)Bonding Molecular Orbitals' Contributions to Chemical Bonding. *Phys. Chem. Chem. Phys.* **2019**, *21* (37), 20988–20998. https://doi.org/10.1039/C9CP04345D.

(46) Neese, F. The ORCA Program System. *WIREs Comput Mol Sci* **2012**, *2* (1), 73–78. https://doi.org/10.1002/wcms.81.

(47) Neese, F. Software Update: The ORCA Program System, Version 4.0. *WIREs Comput Mol Sci* **2018**, *8* (1). https://doi.org/10.1002/wcms.1327.

(48) Cohen, A. J.; Handy, N. C. Dynamic Correlation. *Mol. Phys.* **2001**, *99* (7), 607–615. https://doi.org/10.1080/00268970010023435.

(49) Sastri, C. V.; Lee, J.; Oh, K.; Lee, Y. J.; Lee, J.; Jackson, T. A.; Ray, K.; Hirao, H.; Shin, W.; Halfen, J. A.; Kim, J.; Que, L.; Shaik, S.; Nam, W. Axial Ligand Tuning of a Nonheme Iron(IV) Oxo Unit for Hydrogen Atom Abstraction. *Proceedings of the National Academy of Sciences* **2007**, *104* (49), 19181–19186. https://doi.org/10.1073/pnas.0709471104.

(50) de Oliveira, F. T.; Chanda, A.; Banerjee, D.; Shan, X.; Mondal, S.; Que, L.; Bominaar, E. L.; Munck, E.; Collins, T. J. Chemical and Spectroscopic Evidence for an FeV-Oxo Complex. *Science* **2007**, *315* (5813), 835–838. https://doi.org/10.1126/science.1133417.

(51) Hanwell, M. D.; Curtis, D. E.; Lonie, D. C.; Vandermeersch, T.; Zurek, E.; Hutchison, G. R. Avogadro: An Advanced Semantic Chemical Editor, Visualization, and Analysis Platform. *J Cheminform* **2012**, *4* (1), 17. https://doi.org/10.1186/1758-2946-4-17.

(52) *Avogadro: An Open-Source Molecular Builder and Visualization Tool. Version 1.90.*

(53) Weigend, F. Accurate Coulomb-Fitting Basis Sets for H to Rn. *Phys. Chem. Chem. Phys.* **2006**, *8* (9), 1057. https://doi.org/10.1039/b515623h.

(54) Weigend, F.; Ahlrichs, R. Balanced Basis Sets of Split Valence, Triple Zeta Valence and Quadruple Zeta Valence Quality for H to Rn: Design and Assessment of Accuracy. *Phys. Chem. Chem. Phys.* **2005**, *7* (18), 3297. https://doi.org/10.1039/b508541a.

(55) Poater, J.; Solà, M.; Duran, M.; Fradera, X. The Calculation of Electron Localization and Delocalization Indices at the Hartree-Fock, Density Functional and Post-Hartree-Fock Levels of Theory. *Theoretical Chemistry Accounts: Theory, Computation, and Modeling (Theoretica Chimica Acta)* **2002**, *107* (6), 362–371. https://doi.org/10.1007/s00214-002-0356-8.

Authors are required to submit a graphic entry for the Table of Contents (TOC) that, in conjunction with the manuscript title, should give the reader a representative idea of one of the following: A key structure, reaction, equation, concept, or theorem, etc., that is discussed in the manuscript. Consult the journal's Instructions for Authors for TOC graphic specifications.